RSC Advances

PAPER

View Article Online
View Journal | View Issue

Cite this: *RSC Adv.*, 2017, **7**, 24149

Facile synthesis of MoS_2/reduced graphene oxide composites for efficient removal of Cr(VI) from aqueous solutions†

Xiaolu Jiang,[abc] Hanjin Luo, *[abc] Yuwei Yin[abc] and Weijia Zhou [a]

Cr(VI) as a common heavy metal contaminate has attracted much attention for its high toxicity and bioaccumulation. In this study, novel adsorbents, MoS_2/reduced graphene oxide composites (MoS_2/rGO), were prepared *via* a facile solvothermal process and effectively used for Cr(VI) adsorption. The MoS_2/rGO was characterized by SEM, TEM, XRD, BET and XPS. Results showed that the MoS_2 layers had been successfully grown on the surface of reduced graphene oxide layers. MoS_2/rGO exhibited an enhanced surface area of 81.34 $m^2\ g^{-1}$, more than rGO (57.20 $m^2\ g^{-1}$) and MoS_2 (1.57 $m^2\ g^{-1}$). Batch adsorption experiments of Cr(VI) were also investigated. The pseudo-second order model best described the adsorption kinetics. Effective Cr(VI) removal occurred in a wide pH range from 2.0 to 10.0. The excellent adsorption capacity at 25 °C, calculated from the Langmuir isotherm model, was 268.82 mg g^{-1} at pH 2.0 and 192.63 mg g^{-1} at pH 4.6. The electrostatic attraction and reduction on the adsorbents surface was considered to be the possible mechanism of Cr(VI) removal. These studies revealed the potential application of MoS_2/rGO for Cr(VI) removal.

Received 27th March 2017
Accepted 19th April 2017

DOI: 10.1039/c7ra03531d

rsc.li/rsc-advances

1. Introduction

The removal of heavy metals from wastewater has attracted much attention due to their high toxicity, persistence and non-degradability in the ecosystem. Hexavalent chromium (Cr(VI)) is a widespread environmental and public health problem as it is widely used in metallurgical and chemical industries. Plenty of industrial effluents contain chromium species discharged from leather tanning, paint, steel, electroplating, wood preservation, textile industries, *etc.*[1] It is known that both Cr(III) and Cr(VI) exist in industrial wastewater, while Cr(VI) is about 500 times more toxic than Cr(III) due to its carcinogenic properties. It can be easily adsorbed in the human body through the digestive system, respiratory tract and skin contact.[2]

There are various methods to remove Cr(VI) that have been reported, such as chemical precipitation, ion exchange, electrodeposition, filtration, adsorption, membrane separation, and reduction.[3] Compared to these methods, adsorption is an easy, effective and flexible method for removing Cr(VI). Adsorbents used for Cr(VI) include activated carbon, chitosan, activated alumina, biomaterials, ethyl cellulose, zeolites, and modified graphene.[3–5] Graphene, as a carbon material with a special one-atom thick structure, has received much attention. It has excellent thermal, electrical, optical, and mechanical properties. As reported, graphene is a promising adsorbent for removing heavy metals, dyes and fluoride ions from aqueous solutions.[6] Reduced graphene oxide (rGO) is the product of incomplete reduction of graphene oxide (GO), which containing a number of the oxygen-containing functional groups. The existence of irreversible aggregation during the process of direct GO reduction in water limits the use of rGO for heavy metal adsorption. Molybdenum disulfide (MoS_2) has been investigated in several fields including electrochemical devices, hydrogen storage, catalysis, capacitors, solid lubricants, and intercalation hosts due to its unique chemical and physical properties.[7–9] It is known that MoS_2 has an analogous structure to graphite, which is like a sandwich with a Mo layer between two S layers; these three atom layers stacked together in a through weak van der Waals interactions.[10] As reported, MoS_2 provides a large surface area for double-layer charge storage due to its special sheet-like structure,[11] which may be used for metal ion adsorption. MoS_2 embedded in graphene sheets through a simple hydrothermal method can be helpful for the reduction of overlapping and coalescing of graphene layers, enlarging the specific surface area and increasing the adsorption capacity of the material. The combination of graphene and MoS_2 has already shown to have an excellent electrochemical performance,[12] and it may also produce new properties through their interactions. In this study, we

[a]*School of Environment and Energy, South China University of Technology, Guangzhou Higher Education Mega Centre, Guangzhou 510006, PR China. E-mail: luohj@scut.edu.cn; Fax: +86-20-39380508; Tel: +86-20-87110517*

[b]*The Key Lab of Pollution Control and Ecosystem Restoration in Industry Clusters, Ministry of Education, South China University of Technology, Guangzhou Higher Education Mega Centre, Guangzhou 510006, PR China*

[c]*Guangdong Engineering and Technology Research Center for Environmental Nanomaterials, Guangzhou 510006, PR China*

† Electronic supplementary information (ESI) available. See DOI: 10.1039/c7ra03531d

synthesized MoS_2/rGO by a simple solvothermal process, which was used for removing Cr(VI) from aqueous solutions for the first time. The present study presents a new application of MoS_2/rGO for the removal of Cr(VI) from aqueous solutions.

2. Materials and methods

2.1 Materials

Potassium dichromate ($K_2Cr_2O_7$), thioacetamide (CH_3CSNH_2) and all acid reagents (HNO_3) were of guaranteed grade. Ammonium molybdate ($(NH_4)_6Mo_7O_{24}\cdot 4H_2O$) and the other chemicals and reagents used in the experiments were of analytical grade and used without further purification. All solutions were prepared using deionized water. All stopped conical flasks, beakers, centrifuge tubes, pipettes and containers were carefully cleaned and soaked in 10% HNO_3 for one day, triply rinsed with deionized water and air-dried before use.

2.2 Methods

2.2.1 Preparation of MoS_2/rGO. MoS_2/rGO was prepared *via* a simple hydrothermal process. Briefly, graphene oxide was prepared by a modified Hummers method.[6] Ammonium molybdate and graphene oxide at a mass ratio of 1 : 9, ammonium molybdate and thioacetamide at a mass ratio of 1 : 2, and 1080 mg of ammonium molybdate were dissolved in 40 mL of a 3 mg mL^{-1} graphene oxide aqueous dispersion. After ultrasonication and stirring for 1 h, aqueous NaOH was added until the pH value changed to 6.5. Furthermore, 2160 mg thioacetamide was added and ultrasonicated to form a homogeneous solution; the solution was transferred into a 50 mL Teflon-lined stainless steel autoclave, sealed tightly, and heated at 200 °C for 24 h in an electric oven. For comparison, mass ratios of 1 : 1, 1 : 3, 1 : 5, 1 : 7, pure MoS_2 and rGO were prepared in the same manner.

2.2.2 Characterization of MoS_2/rGO. MoS_2/rGO was observed with a Merlin field emission scanning electron microscope (SEM) equipped with energy dispersive spectroscopy (EDS) and a FEI Tecnai G2 F20 transmission electron microscope (TEM) with high-resolution transmission electron microscopy (HRTEM). XRD patterns of MoS_2/rGO were collected using a D8-Advance X-ray diffractometer based on Cu Kα radiation. The Brunauer–Emmett–Teller (BET) surface area of MoS_2/rGO was determined using a Quantachrome Autosorb-IQ-MP low temperature nitrogen sorption method. The XPS spectrum was recorded on the Thermo Fisher Scientific ESCALAB 250Xi spectrometer with monochromatic Al Kα radiation.

2.2.3 Cr(VI) adsorption experiments. For batch adsorption experiments of Cr(VI), a stock solution of Cr(VI) at concentration of 1000 mg L^{-1} was prepared. All adsorption experiments were conducted at room temperature (25 ± 2 °C) at an agitation speed of 180 rpm and the normal pH of Cr(VI) solutions (4.6 ± 0.1) unless otherwise noted. Adsorption kinetics were studied by adding 0.01 g of adsorbents into 25 mL of 50 mg L^{-1} Cr(VI) solutions and stirring for specific time intervals. The effect of the adsorbent dose was analyzed by a dosing range from 0.005 g to 0.025 g. To observe the pH effect on the adsorption, Cr(VI) solutions with varying pH values from 2.0 (±0.1) to 10.0 (±0.1) were prepared. The effect of the initial Cr(VI) concentration was investigated from 10 mg L^{-1} to 100 mg L^{-1}. Adsorption isotherm studies were performed at different temperatures from 25 °C to 45 °C. All experiments were repeated three times. After shaking, the samples were filtered with a 0.45 μm filter membrane. The filtrate was used for the remaining Cr(VI) determination, and the Cr(VI) removal and adsorption capacity were determined by triplicate measurements, with the average data reported.

2.2.4 Determination of Cr(VI) concentration. The concentration of Cr(VI) was analyzed by a UV-Vis spectrophotometer (UV-1750, SHIMADZU, Japan), which was measured by the purple complex of Cr(VI) with 1,5-diphenylcarbazide at 540 nm.[2] The details of the analytical method are presented in ESI.†

3. Results and discussions

3.1 Characterization of materials

The morphology of MoS_2/rGO was observed by SEM and is shown in Fig. 1. The SEM image of MoS_2/rGO clearly illustrates a 3D sphere-like architecture, which is quite different from the reported flake-like structure of graphene. The interaction of MoS_2 and rGO resulted in the overlapping or coalescence of graphene layers being more difficult; thus the 3D sphere-like architecture increased the specific surface area and aided the adsorption. Due to the superior strength of graphene, the 3D sphere-like architecture was also helpful for the stability of MoS_2/rGO.[13]

The TEM image of MoS_2/rGO is shown in Fig. 2. From Fig. 2, it is clear that the MoS_2 (black stripes) layers are homogeneously embedded in the graphene layers. The thickness of pure MoS_2 is reported to be tens of layers,[14] while the thickness of MoS_2 embedded in graphene layers, shown in the HRTEM image, is smaller than pure MoS_2 and about 4–5 layers. The difference in thickness reveals that during the self-assembled process of MoS_2/rGO, MoS_2 is grown *in situ* on the surface of the graphene layers, and the combination of MoS_2 and graphene greatly inhibits the restacking of MoS_2 and graphene layers.[14]

Fig. 3 shows the XRD patterns of rGO, MoS_2 and MoS_2/rGO. The XRD pattern of rGO exhibits a clear diffraction peak at $2\theta = 24.8^\circ$, corresponding to the characteristic of graphene. At about $2\theta = 12.3^\circ$, there is a diffraction peak that may be characteristic of graphene oxide because of the incomplete elimination of oxygen-containing functional groups during the synthesis of MoS_2/rGO. The XRD patterns of MoS_2 and MoS_2/rGO show a similar trend because of the big mass ratio of MoS_2 in the composites. The diffraction peak of MoS_2/rGO shows very weak, at (100), (110) diffraction line is slightly stronger than the diffraction peak of MoS_2, indicating the poor crystallinity of MoS_2 and MoS_2/rGO.

The rGO, MoS_2 and MoS_2/rGO were investigated by the BET method to calculate the specific surface area. The nitrogen adsorption/desorption isotherms are shown in Fig. 4. The specific surface area of rGO, MoS_2 and MoS_2/rGO is 57.20 m^2 g^{-1}, 1.57 m^2 g^{-1} and 81.34 m^2 g^{-1}, respectively. The specific surface area of MoS_2/rGO is higher than those of both rGO and

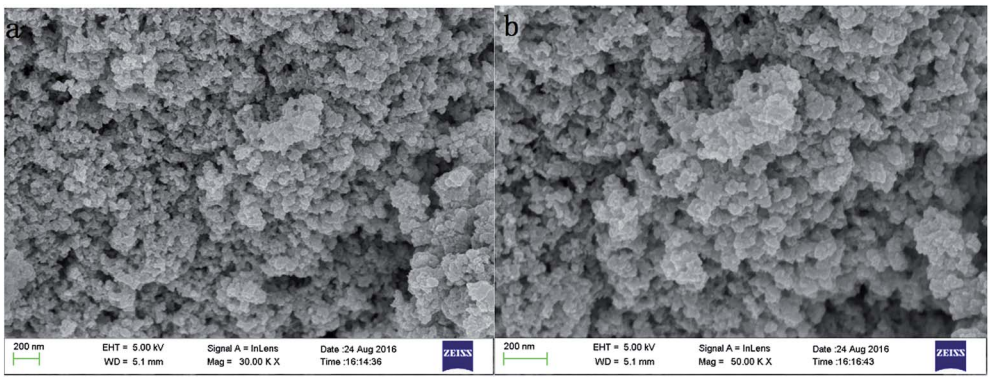

Fig. 1 The SEM image of MoS_2/rGO.

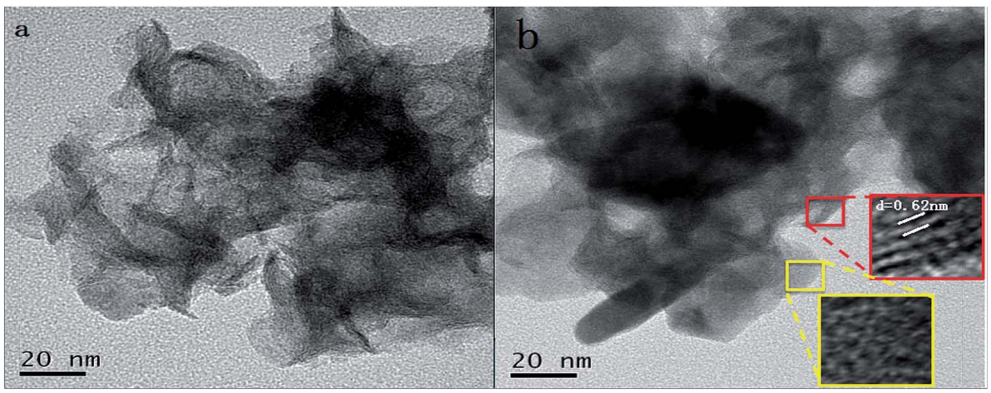

Fig. 2 The TEM and HRTEM images of MoS_2/rGO.

MoS_2, meaning the combination of MoS_2 and rGO can greatly reduce the restacking of MoS_2 layers and graphene layers.

To further understand the chemical composition and valence states of MoS_2/rGO, the XPS spectrum was recorded and shown in Fig. 5. The C 1s peak associated with the binding energy of 284.8 eV represents the sp^2 carbon of graphene (oxide). Two peaks at 229.2 eV and 232.4 eV can be assigned to Mo $3d_{5/2}$ and Mo $3d_{3/2}$, respectively. The S 2p and S 2s can be fitted with the peaks at 162.3 eV, 163.2 eV and 227.5 eV.

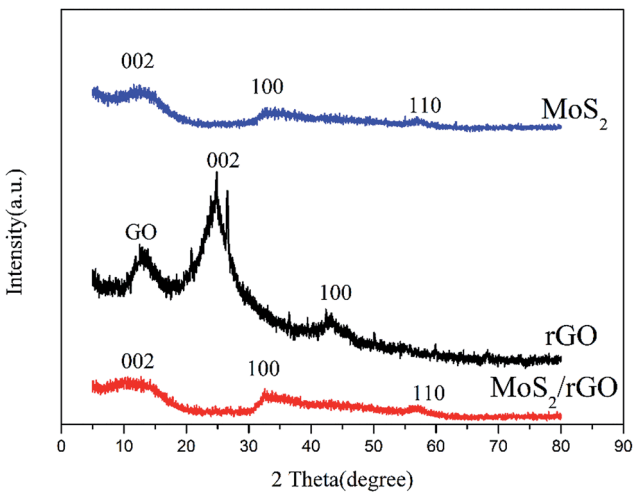

Fig. 3 The XRD patterns of MoS_2, rGO, and MoS_2/rGO.

3.2 Effect of contact time

Fig. 6 shows the effect of contact time on the adsorption of Cr(VI) onto MoS_2/rGO. The adsorption of different initial concentrations of Cr(VI) solutions showed a similar trend. The adsorption capacity at an initial concentration of 50 mg L^{-1} was better than 30 mg L^{-1} and 70 mg L^{-1}. In the first 15 min, the adsorption rapidly increased, which was due to the abundant, available vacant sites of MoS_2/rGO. With further increases in time, the rate of adsorption slowed and reached equilibrium within 180 min. Moreover, the rapid adsorption process is an important feature of physical adsorption, which revealed that the adsorption of Cr(VI) onto MoS_2/rGO is a combination of physical adsorption and chemical adsorption. The optimum contact time was 180 min according to the above results.

3.3 Effect of the adsorbent dose

The relation between the adsorbent dose of MoS_2/rGO and removal efficiency is shown in Fig. 7. With an increase in the MoS_2/rGO dosage, the efficiency of the removal of Cr(VI) increased. In addition, the adsorption capacity decreased. It is

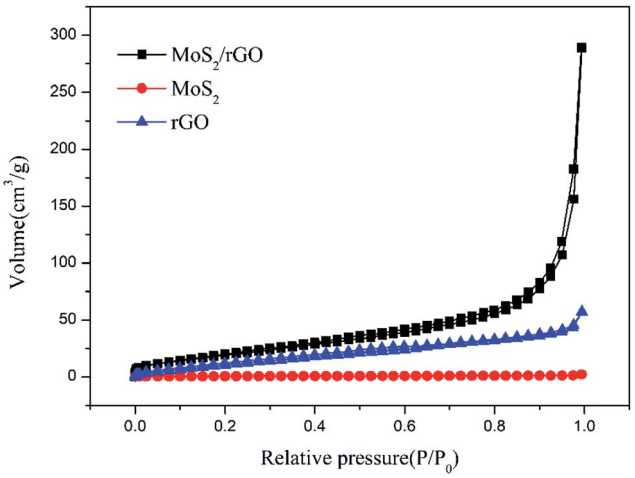

Fig. 4 The nitrogen adsorption/desorption isotherms of rGO, MoS_2 and MoS_2/rGO.

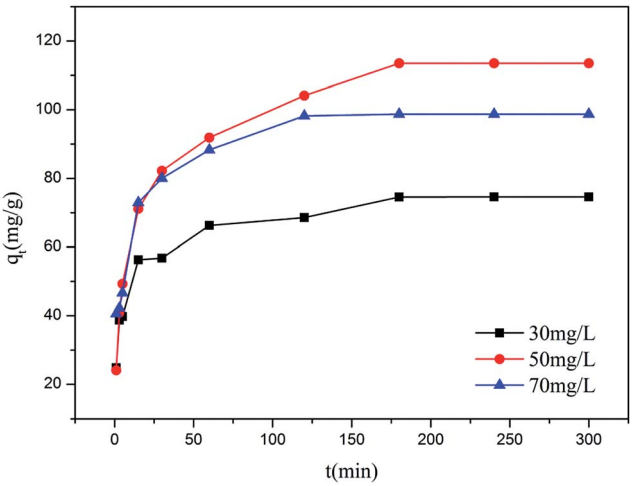

Fig. 6 Effect of contact time on the adsorption of Cr(VI) by MoS_2/rGO.

clear that the efficiency of the removal of Cr(VI) sharply increased from 59.55% to 98.14%, when the adsorbent dose increased from 0.20 g L^{-1} to 0.40 g L^{-1}. Correspondingly, the adsorption capacity decreased from 148.88 mg g^{-1} to 122.67 mg g^{-1}. This might be due an increased dose that led to an enhancement in the surface and the available active sites for adsorption.[15] Based on these results, 0.40 g L^{-1} was selected as an optimum adsorbent dose.

3.4 Effect of pH

Fig. 8 shows the effect of pH on the adsorption of Cr(VI) by MoS_2/rGO. The pH of the solution was an important factor in the adsorption. It indicates that the change between the initial pH of the solution and adsorption capacity of Cr(VI) tends to be similar. At a pH range of 2.0–10.0, MoS_2/rGO (mass ratio of 1 : 9) had a much higher adsorption capacity (>87.59 mg g^{-1}) than the others in this study. MoS_2/rGO (mass ratio of 1 : 9) showed

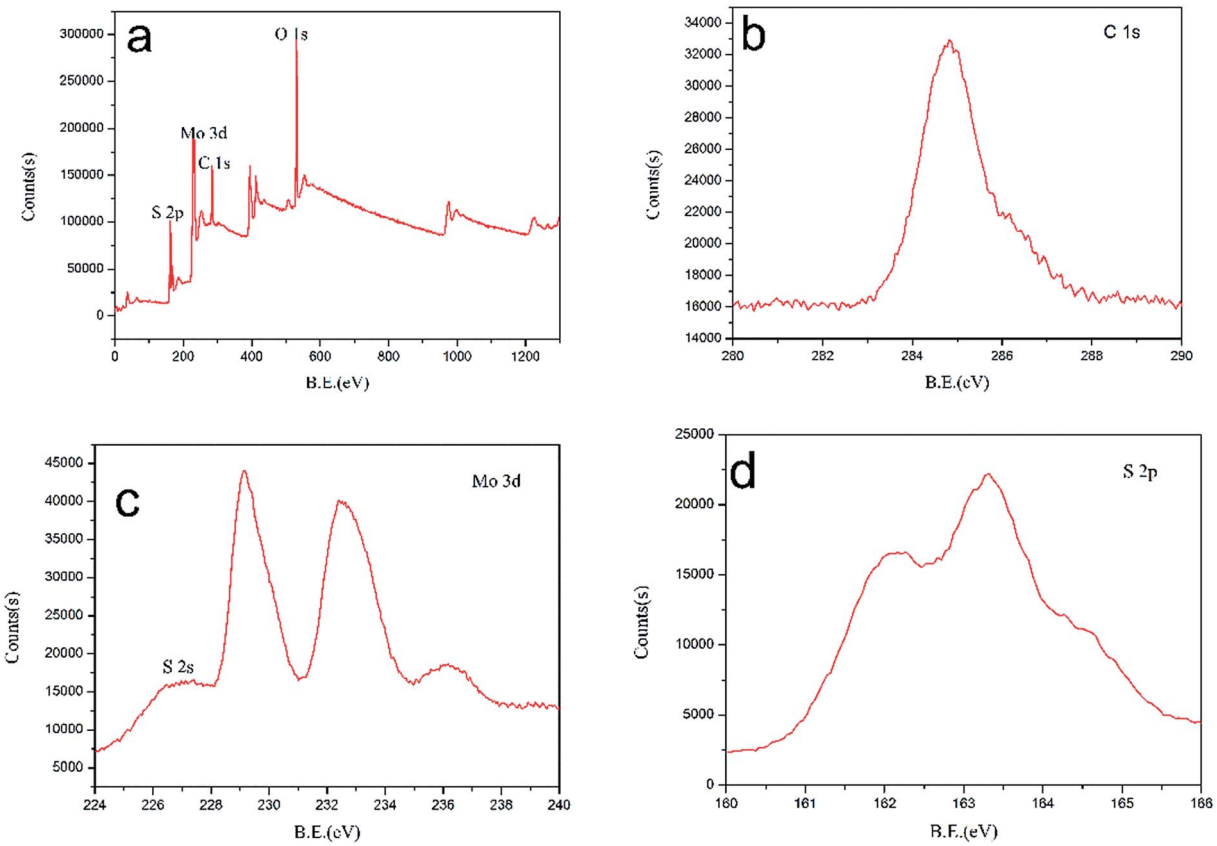

Fig. 5 (a) XPS survey spectrum of MoS_2/rGO and high resolution scans for (b) the C 1s, (c) Mo 3d, and (d) S 2p.

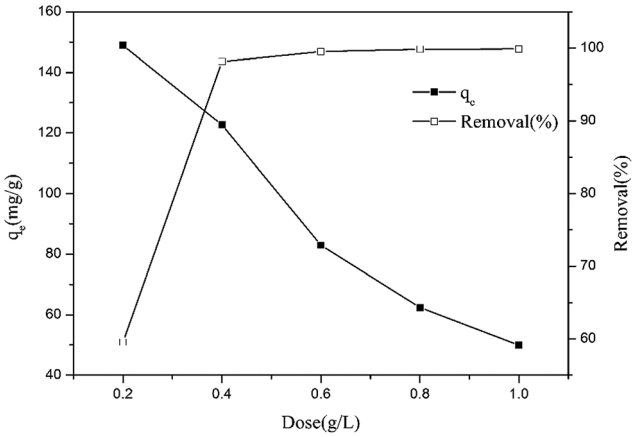

Fig. 7 Effect of adsorption dose on adsorption capacity and removal of Cr(VI) by MoS_2/rGO.

a great adsorption capacity not only at pH 2.0 (124.67 mg g^{-1}) but also at pH 4.6 (118.31 mg g^{-1}). The adsorption capacity decreased with the value of pH increasing until the pH value was 10. Cr(VI) exists in various different ionic forms in solutions. Chromate (CrO_4^{2-}), dichromate ($Cr_2O_7^{2-}$) and hydrogen chromate ($HCrO_4^-$) are the main ionic forms of Cr(VI) in solutions. At a pH lower than 6.8, $HCrO_4^-$ is the major species, while above 6.8, only CrO_4^{2-} is stable. Under acidic conditions, the adsorption is facilitated by electrostatic attraction between the sorbents and sorbates, which might due to the protonation on the sorbents surface. In fact, much chromium-containing water is acidic, such as electroplating wastewater at pH 4–6 and acid pickling wastewater at a pH lower than 1.5. Most of the reported adsorbents of Cr(VI) show a high adsorption capacity only under strong acidic conditions, such as pH 2.0. In this case, pH 4.6 was selected for the subsequent experiments unless otherwise noted. This was done to avoid adjusting the pH value of Cr(VI) solutions to reduce experimental error and to show the great potential of MoS_2/rGO for removing Cr(VI) compared to the other reported adsorbents at pH 4.6.

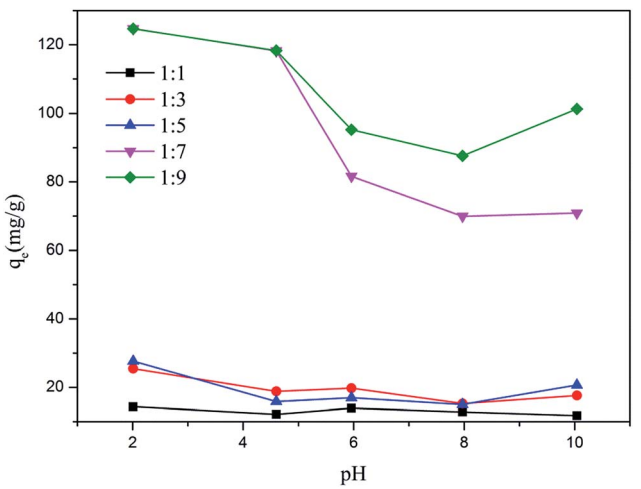

Fig. 8 Effect of pH on the adsorption of Cr(VI) by MoS_2/rGO.

3.5 Effect of initial concentration

The effect of the initial concentration on Cr(VI) adsorption by rGO, MoS_2 and MoS_2/rGO is shown in Fig. 9. It shows that the adsorption capacity of MoS_2/rGO is quite higher than the adsorption capacity of rGO and MoS_2, signifying that the combination of rGO and MoS_2 not only exhibited the properties of constituents, but also produced new properties through the interaction.

3.6 Adsorption kinetics study

The pseudo-first order[16] model and the pseudo-second order[17] model were employed to investigate the controlling mechanism. The linearized forms of the adsorption kinetic models are given in eqn (1) and (2), respectively:

$$\log(q_e - q_t) = \log q_e - \frac{k_1}{2.303} t \quad (1)$$

$$\frac{t}{q_t} = \frac{1}{k_2 q_e^2} + \frac{t}{q_e} \quad (2)$$

where q_e is the amount adsorbed at equilibrium (mg g^{-1}), q_t is the amount adsorbed at time t (mg g^{-1}), and k_1 and k_2 are the pseudo-first order and pseudo-second order, respectively.

Fig. 10a and b show the linearized plots of eqn (1) and (2), respectively. The fitting results of kinetic models are shown in Table 1. The results suggest that the calculated q_e values by a pseudo-second order model are close to the experimental values and the correlation coefficient ($r^2 \approx 0.9990$–0.9996). Meanwhile, the calculated q_e values by a pseudo-first order model greatly differ from the experimental values, and the correlation coefficient ($r^2 \approx 0.6363$–0.9455), which indicates that the Cr(VI) adsorption onto MoS_2/rGO fits well with the pseudo-second order model than the pseudo-first order model.

3.7 Adsorption isotherms study

The Langmuir[18] and Freundlich[19] isotherm models were employed to understand the adsorption mechanism. The

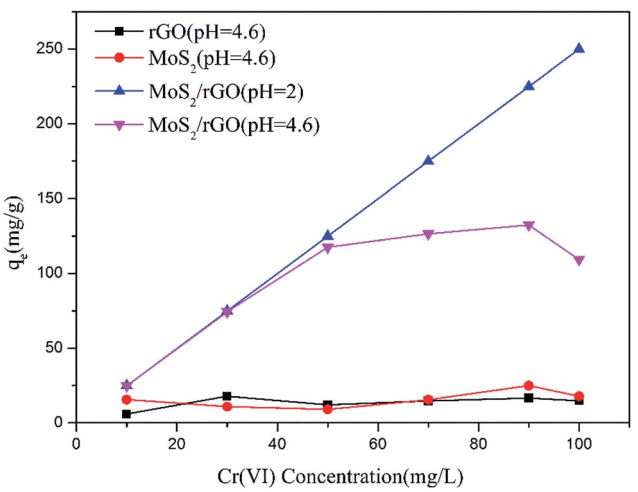

Fig. 9 Effect of initial concentration on the adsorption of Cr(VI) by rGO, MoS_2 and MoS_2/rGO.

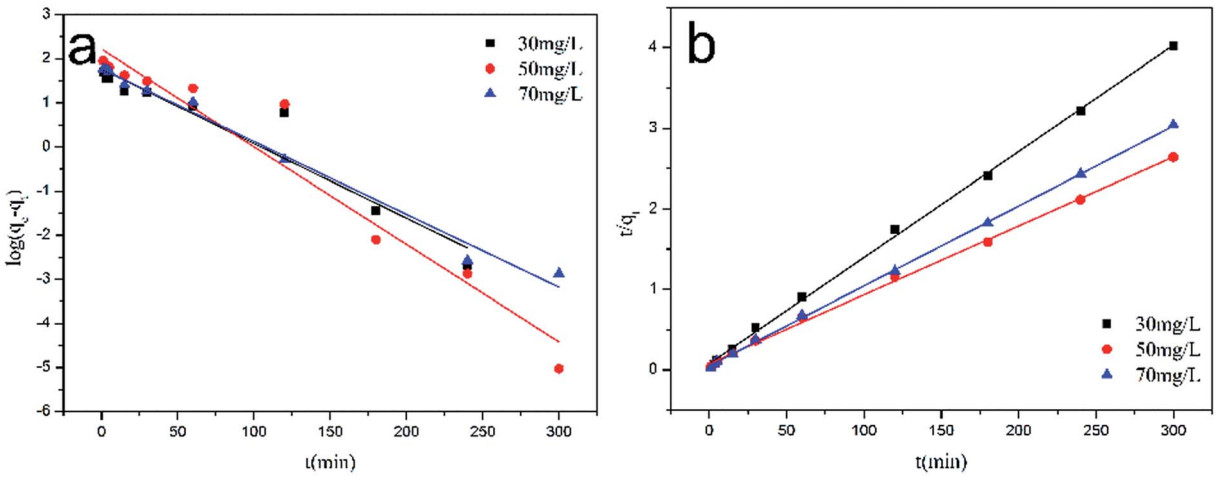

Fig. 10 (a) The pseudo-first-order, (b) the pseudo-second-order kinetics model for the adsorption of Cr(VI) by MoS_2/rGO.

Table 1 Kinetic parameters for the adsorption of Cr(VI) by MoS_2/rGO

		Parameters			
Kinetic models		$q_{e,exp}$ (mg g^{-1})	$q_{e,cal}$ (mg g^{-1})	k_1 (min^{-1})	r^2
Pseudo-first-order model	30 mg L^{-1}	74.59	31.83	2.46×10^{-2}	0.6363
	50 mg L^{-1}	113.49	164.38	5.09×10^{-2}	0.9461
	70 mg L^{-1}	98.74	63.92	3.59×10^{-2}	0.9455
		Parameters			
Kinetic models		$q_{e,exp}$ (mg g^{-1})	$q_{e,cal}$ (mg g^{-1})	k_2 [g mg^{-1} min^{-1}]	r^2
Pseudo-second-order model	30 mg L^{-1}	74.59	75.87	0.22×10^{-2}	0.9990
	50 mg L^{-1}	113.49	116.82	0.09×10^{-2}	0.9985
	70 mg L^{-1}	98.74	100.70	0.20×10^{-2}	0.9996

Langmuir isotherm assumes a homogeneous adsorption surface with all the adsorption sites having an equal adsorbate affinity. The equation of the Langmuir isotherm is given as follows:

$$\frac{c_e}{q_e} = \frac{c_e}{q_m} + \frac{1}{k_L q_m} \quad (3)$$

where q_m is the maximum adsorption capacity (mg g^{-1}), and k_L is the Langmuir constant related to the free energy of

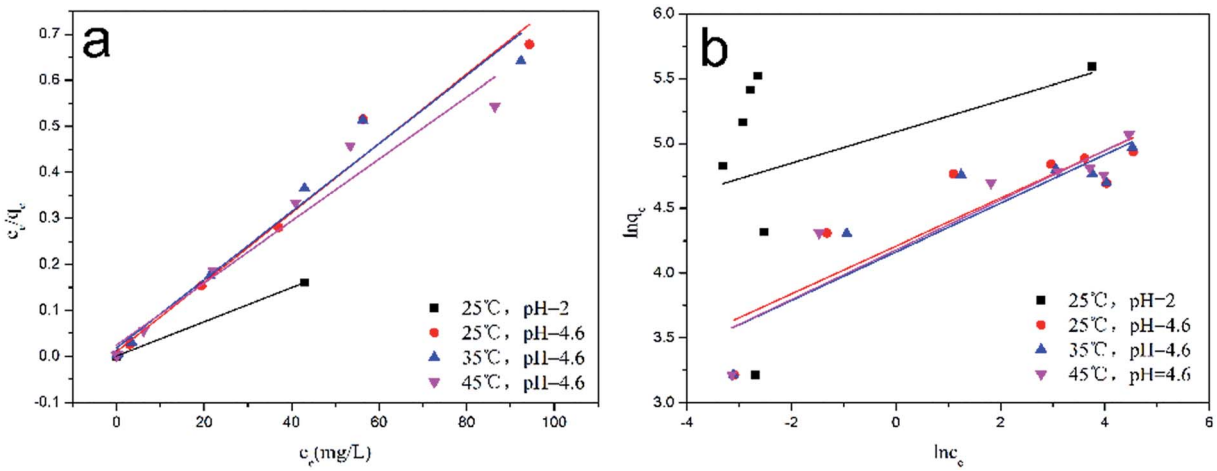

Fig. 11 (a) The Langmuir, and (b) the Freundlich isotherm models for the adsorption of Cr(VI) by MoS_2/rGO.

adsorption. In addition, a dimensionless separation constant R_L can be expressed as follows:

$$R_L = \frac{1}{1 + k_L c_0} \quad (4)$$

where the value of R_L indicates the type of isotherm that is unfavorable ($R_L > 1$), linear ($R_L = 1$), favorable ($0 < R_L < 1$), or irreversible ($R_L = 0$).

The Freundlich isotherm assumes a heterogeneous adsorption surface during the adsorption process. The Freundlich isotherm model is represented by the following equation:

$$\ln q_e = \frac{1}{n} \ln c_e + \ln k_F \quad (5)$$

where $1/n$ and k_F are the constants related to the intensity of adsorption and capacity of adsorption, respectively.

Fig. 11a and b show the linearized plots of the Langmuir and Freundlich isotherm models, and the values of the parameters are listed in Table 2. Based on the high value of the correlation coefficient by the Langmuir isotherm model ($r^2 \approx 0.9998$–0.9601) compared to the Freundlich isotherm model ($r^2 \approx 0.1247$–0.8377), the Langmuir isotherm model gave a better description of Cr(VI) adsorption by MoS_2/rGO. The maximum capacity at pH 2.0 and pH 4.6 at 25 °C were calculated to be 268.82 mg g^{-1} and 192.63 mg g^{-1}, respectively. The value of R_L at three different temperatures was in the range of 0.0011–0.0234 and revealed that the Cr(VI) adsorption process was favorable. The comparison of the maximum adsorption capacity of MoS_2/rGO with various reported adsorbents in the Langmuir isotherm is shown in Table 3. The dose of MoS_2/rGO was only 0.4 g L^{-1}, which is much less than some materials, such as reduced graphene oxide–montmorillonite[3] (6.0 g L^{-1}) and polypyrrole/F_3O_4 magnetic nanocomposite[5] (2.0 g L^{-1}), among others.[6,20–22] Based on the results, the MoS_2/rGO had a much higher maximum adsorption capacity than others, which can be considered as a promising material for the removal of Cr(VI) in wastewater.

3.8 Thermodynamic study

To investigate the thermodynamic study of MoS_2/rGO, the Gibbs free energy (ΔG^0), enthalpy (ΔH^0), and entropy (ΔS^0)[23] were determined at temperatures from 298 K to 318 K, as shown in Table 4. At all three temperatures, the negative value of ΔG^0 indicated that the Cr(VI) adsorption process by MoS_2/rGO was spontaneous. The negative ΔH^0 value suggested that the removal of Cr(VI) was an exothermic reaction.[24]

3.9 Adsorption mechanism

The EDS pattern (Fig. 12a) of MoS_2/rGO after Cr(VI) adsorption at pH 4.6 revealed the existence of C, O, Mo, S and Cr. Furthermore, it was noted that the peaks of Mo and S were overlapped. To further understand the adsorption mechanism of MoS_2/rGO, Cr ions loaded on the surface of MoS_2/rGO after Cr(VI) adsorption at pH 4.6 were employed to XPS. The XPS spectra are shown in Fig. 12b. There are two obvious energy bands at about 577.5 eV and 587.5 eV, which correspond to the orbital binding energies

Table 4 Thermodynamic parameters for the adsorption of Cr(VI) by MoS_2/rGO

T (K)	ΔG^0 (kJ mol^{-1})	ΔH^0 (kJ mol^{-1})	ΔS^0 (J mol^{-1} K^{-1})
298	−7.0085	−30.7309	−79.6053
308	−6.2124		
318	−5.4164		

Table 2 Isotherm parameters for the adsorption of Cr(VI) by MoS_2/rGO

		Langmuir					Freundlich	
Temp (°C)	pH	q_m (mg g^{-1})	k_L (L mg^{-1})	r^2	R_L	$1/n$	k_F (mg g^{-1})	r^2
25	2.0	268.82	6.2000	0.9998	0.0011	0.1209	162.4061	0.1247
	4.6	192.63	0.7414	0.9799	0.0089	0.1842	67.2805	0.7730
35	4.6	134.95	0.4074	0.9720	0.0161	0.1874	64.3599	0.8030
45	4.6	148.15	0.2787	0.9601	0.0234	0.1917	65.3149	0.8377

Table 3 Comparison of adsorption capacity for Cr(VI) on different adsorbents at 25 °C

Adsorbent	Dose (g L^{-1})	pH	q_{max} (mg g^{-1})	Reference
MoS_2/rGO	0.4	2.0	268.82	This study
MoS_2/rGO	0.4	4.6	192.63	This study
Reduced graphene oxide–montmorillonite	6.0	2.0	12.86	3
Polypyrrole/F_3O_4 magnetic nanocomposite	2.0	2.0	169.4–243.9	5
Graphene modified with cetyltrimethylammonium bromide	4.0	2.0	21.57	6
Graphene oxide/Fe_3O_4/SO_3H nanohybrid	0.5	3.0	222.22	20
Magnetic ionic liquid/chitosan/graphene oxide composite	1.0	3.0	145.35	21
β-Cyclodextrin–chitosan modified biochars	2.0	2.0	206	22

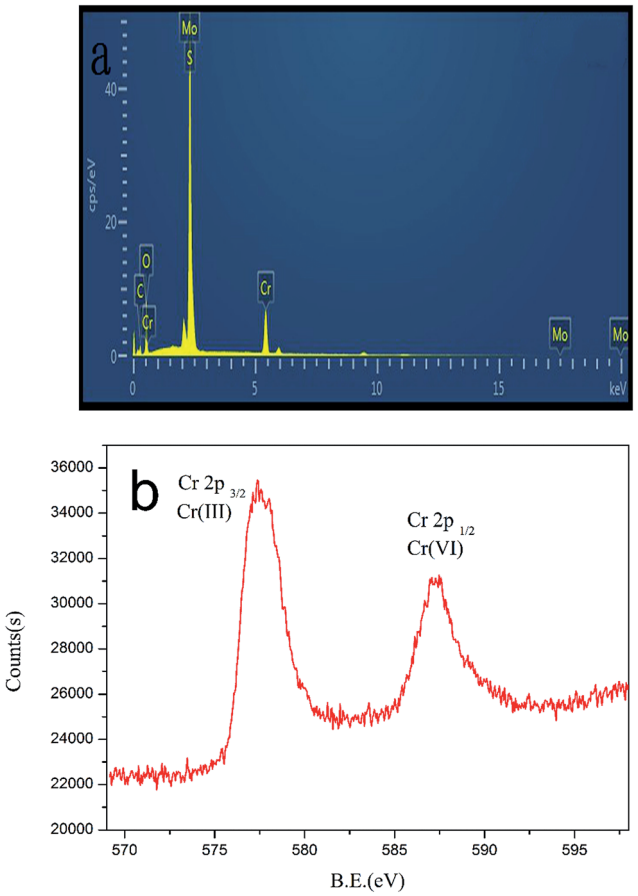

Fig. 12 (a) EDS pattern and (b) XPS spectra of the MoS_2/rGO after Cr(VI) adsorption at pH 4.6.

of Cr($2p_{3/2}$) and Cr($2p_{1/2}$), respectively. This indicated that the Cr ions exist as Cr(VI) and Cr(III) on the MoS_2/rGO surface.[5] The Cr(VI) on the adsorbents surface, due to the sorption of Cr(VI), may be due to the specific surface area of MoS_2/rGO and the electrostatic attraction between adsorbents and Cr(VI) ions. The Cr(III) on the adsorbents surface suggests that some fraction of adsorbed Cr(VI) on the MoS_2/rGO surface is reduced to Cr(III), and the Cr(III) species can be precipitated on the surface of MoS_2/rGO due to the co-electron cloud, which formed by the electrons of the S atom layer and its adjacent carbon layer.[18] The reduction was accompanied by the consumption of protons (eqn (6)).

$$HCrO_4^- + 7H^+ + 3e^- \rightarrow Cr^{3+} + 4H_2O \quad (6)$$

4. Conclusions

In this study, MoS_2/rGO was synthesized *via* a facile, one-step solvothermal process and successfully showed new properties for Cr(VI) removal. It had an excellent adsorption capacity from pH 2.0 to 10.0 compared to some of the reported adsorbents. The adsorption kinetics fitted better to a pseudo-second-order model than a pseudo-first-order model. The Langmuir isotherm was found to describe the experimental data better than the Freundlich isotherm. The maximum adsorption capacity of MoS_2/rGO at pH 2.0 and at pH 4.6 was 268.82 mg g^{-1} and 192.63 mg g^{-1}, respectively. A thermodynamic study suggested that Cr(VI) adsorption was spontaneous and exothermic. The abovementioned results revealed that MoS_2/rGO can be an effective adsorbent for the removal of Cr(VI).

Acknowledgements

Financial support from the Key Natural Science Foundation of Guangdong Province (No. 2015A030311002) is gratefully acknowledged.

References

1 T. Karthikeyan, S. Rajgopal and L. Miranda, *J. Hazard. Mater.*, 2005, **124**, 192.
2 B. Hu and H. Luo, *Appl. Surf. Sci.*, 2010, **257**, 769.
3 Z. Zhang, H. Luo, X. Jiang, Z. Jiang and C. Yang, *RSC Adv.*, 2015, **5**, 47408.
4 Y. Zhao, H. Shen, S. Pan, M. Hu and Q. Xia, *J. Mater. Sci.*, 2010, **45**, 5291.
5 M. Bhaumik, A. Maity, V. V. Srinivasu and M. S. Onyango, *J. Hazard. Mater.*, 2011, **190**, 381.
6 Y. Wu, H. Luo, H. Wang, C. Wang, J. Zhang and Z. Zhang, *J. Colloid Interface Sci.*, 2013, **394**, 183.
7 J. Chen, N. Kuriyama, H. Yuan, H. T. Takeshita and T. Sakai, *J. Am. Chem. Soc.*, 2001, **47**, 11813.
8 S. J. Ding, J. S. Chen and X. W. Lou, *Chem.–Eur. J.*, 2011, **17**, 13142.
9 M. Sun, J. Adjaye and A. E. Nelson, *Appl. Catal., A*, 2004, **263**, 131.
10 H. S. S. Ramakrishna Matte, A. Gomathi, A. K. Manna, D. J. Late, R. Datta, S. K. Pati and C. N. R. Rao, *Angew. Chem.*, 2010, **122**, 4153.
11 J. M. Soon and K. P. Loh, *Electrochem. Solid-State Lett.*, 2007, **10**, A250.
12 W. Zhou, K. Zhou, D. Hou, X. Liu, G. Li, Y. Sang, H. Liu, L. Li and S. Chen, *ACS Appl. Mater. Interfaces*, 2014, **6**, 21534.
13 K. Huang, L. Wang, Y. Liu, Y. Liu, H. Wang, T. Gan and L. Wang, *Int. J. Hydrogen Energy*, 2013, **38**, 14027.
14 K. Chang and W. Chen, *Chem. Commun.*, 2011, **47**, 4252.
15 E. N. El Qada, S. J. Allen and G. M. Walker, *Ind. Eng. Chem. Res.*, 2006, **45**, 6044.
16 M. Doğan, M. Alkan, Ö. Demirbaş, Y. Özdemir and C. Özmetin, *Chem. Eng. J.*, 2006, **124**, 89.
17 Y. S. Ho and C. C. Chiang, *Adsorption*, 2001, **7**, 139.
18 I. Langmuir, *J. Am. Chem. Soc.*, 1918, **40**, 1361.
19 H. M. F. Freundlich, *J. Phys. Chem.*, 1906, **57**, 385.
20 A. Alizadeh, G. Abdi, M. M. Khodaei, M. Ashokkumarc and J. Amiriand, *RSC Adv.*, 2017, **7**, 14876.
21 L. Li, C. Luo, X. Li, H. Duan and X. Wang, *Int. J. Biol. Macromol.*, 2014, **66**, 172.
22 X. Huang, Y. Liu, S. Liu, X. Tan, Y. Ding, G. Zeng, Y. Zhou, M. Zhang, S. Wang and B. Zheng, *RSC Adv.*, 2016, **6**, 94.
23 L. Zhang, H. Luo, P. Liu, W. Fang and J. Geng, *Int. J. Biol. Macromol.*, 2016, **87**, 586.
24 N. Nasuha and B. H. Hameed, *Chem. Eng. J.*, 2011, **166**, 783.